1582 *Biochemistry* **2011,** *50,* 1582–1589
DOI: 10.1021/bi1018545

BIOCHEMISTRY
including biophysical chemistry & molecular biology
Article

Effect of Osmolytes on Protein Dynamics in the Lactate Dehydrogenase-Catalyzed Reaction[†]

Nickolay Zhadin and Robert Callender*

Department of Biochemistry, Albert Einstein College of Medicine, Bronx, New York 10461, United States

Received November 19, 2010; Revised Manuscript Received January 20, 2011

ABSTRACT: Laser-induced temperature jump relaxation spectroscopy was used to probe the effect of osmolytes on the microscopic rate constants of the lactate dehydrogenase-catalyzed reaction. NADH fluorescence and absorption relaxation kinetics were measured for the lactate dehydrogenase (LDH) reaction system in the presence of varying amounts of trimethylamine *N*-oxide (TMAO), a protein-stabilizing osmolyte, or urea, a protein-destabilizing osmolyte. Trimethylamine *N*-oxide (TMAO) at a concentration of 1 M strongly increases the rate of hydride transfer, nearly nullifies its activation energy, and also slightly increases the enthalpy of hydride transfer. In 1 M urea, the hydride transfer enthalpy is almost nullified, but the activation energy of the step is not affected significantly. TMAO increases the preference of the closed conformation of the active site loop in the LDH·NAD^+·lactate complex; urea decreases it. The loop opening rate in the LDH·NADH·pyruvate complex changes its temperature dependence to inverse Arrhenius with TMAO. In this complex, urea accelerates the loop motion, without changing the loop opening enthalpy. A strong, non-Arrhenius decrease in the pyruvate binding rate in the presence of TMAO offers a decrease in the fraction of the open loop, pyruvate binding competent form at higher temperatures. The pyruvate off rate is not affected by urea but decreases with TMAO. Thus, the osmolytes strongly affect the rates and thermodynamics of specific events along the LDH-catalyzed reaction: binding of substrates, loop closure, and the chemical event. Qualitatively, these results can be understood as an osmolyte-induced change in the energy landscape of the protein complexes, shifting the conformational nature of functional substates within the protein ensemble.

Some osmolytes, such as trimethylamine *N*-oxide (TMAO),[1] are known to protect proteins against harsh environments (*1*, *2*). In particular, TMAO counteracts the destabilizing effect of urea on protein structure (*3*−*5*). Addition of TMAO to a protein solution usually results in increased protein stability against denaturation (*6*, *7*), and higher rigidity of the protein backbone (*8*, *9*). Mechanistically, TMAO compacts a protein globule, while urea does the opposite (*8*, *10*, *11*).

TMAO and urea affect enzymatic activity: urea has been reported to increase K_m and decrease k_{cat} values for many enzymes, while TMAO produced the opposite effect (see refs *1*, *10*, *12*, and *13* and references cited therein). However, these parameters are composed of multiple rate constants, and it is difficult to determine what elementary events are being affected by the osmolytes and how. Hence, our knowledge of dynamic aspects of enzyme function in the presence of osmolytes is quite limited. Previously, we studied the influence of osmolytes on binding of substrate mimics to triosephosphate isomerase (*14*) and lactate dehydrogenase (*15*), to learn how TMAO and urea affected the elementary rate constants along the binding pathway. Here we report on the effects of these two osmolytes on the rate constants for a full, functional enzyme reaction system, the lactate dehydrogenase (LDH) system. The goals were to obtain specific information about the details and mechanism of TMAO and urea action on the enzyme functional dynamics and improve our understanding of the dynamical nature of LDH-catalyzed reaction.

Pig heart L-lactate dehydrogenase (EC 1.1.1.27) catalyzes oxidation of lactate by NAD^+ to produce pyruvate and NADH. The binding of the two substrates is ordered. The substrate binding pocket lies deep within the protein, buried ∼10 Å from the protein's surface. The reaction proceeds in several sequential steps. From the lactate side of the reaction, NAD^+ cofactor binding is followed by lactate substrate binding. The rate-limiting step in the turnover of LDH is not the chemical hydride transfer step but rather loop motion involving closure of the so-called "mobile loop" (surface residues 98−110), occurring in ∼1−10 ms. After that, structural and chemical rearrangements proceed, including in particular a direct stereospecific transfer of a hydride ion from the C2 atom of lactate to the C4 atom of NAD^+, and the transfer of a proton from the lactate hydroxyl to the N3 atom of His-195 (*16*−*18*). This is followed by pyruvate release, and final NADH dissociation. The rate constants associated with these reaction steps (*15*, *19*−*22*) and the whole reaction system (*23*) were investigated in our previous studies using laser-induced temperature jump spectroscopy with nanosecond time resolution. In this study, we continue this series of work, investigating the effect of TMAO and urea on the individual steps of the LDH-catalyzed reaction: hydride transfer, active site mobile loop dynamics, and pyruvate binding and unbinding.

MATERIALS AND METHODS

Laser-Induced Temperature Jump. Laser-induced temperature jump relaxation spectroscopy (system schematic shown

[†]This work was supported by the National Institute of General Medical Sciences of the National Institutes of Health (Grant 5P01GM068036) and the National Institute of Biomedical Imaging and Bioengineering (Grant EB01958).

*To whom correspondence should be addressed. Telephone: (718) 430-3024. Fax: (718) 430-8565. E-mail: robert.callender@einstein.yu.edu.

[1]Abbreviations: LDH, lactate dehydrogenase; TMAO, trimethylamine *N*-oxide; TEA, triethanolamine; FWHM, full width at half-maximum; KIE, kinetic isotope effect.

 Published on Web 02/09/2011

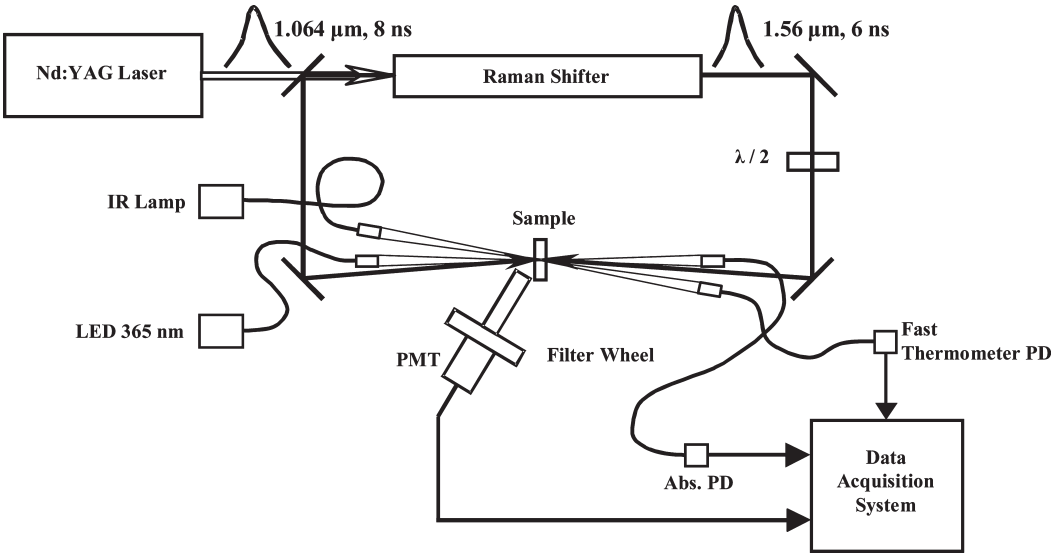

FIGURE 1: Laser-induced temperature jump spectrometer. Collimators in the absorption and fast thermometer channels are coupled to the light sources and photodiodes (PD) by optical fibers. Both output beams from the Raman shifter are directed to the sample from the opposite sides. Polarization of one beam is 90° rotated to avoid a standing wave and Bragg grating formation in the sample.

in Figure 1) is employed in these studies. The sample temperature is rapidly increased with an intense laser pulse absorbed by water-based buffer. Following this nanosecond change in the sample temperature, the system relaxes to a new equilibrium. The relaxation kinetics are followed here by the resulting changes in optical absorption and/or fluorescence emission. To produce the IR pulse necessary for heating, the fundamental (1064 nm) of the YG981C10 Q-switched Nd:YAG laser (Quantel, Bozeman, MT) is Raman-shifted to a wavelength of 1561 nm, to a weak absorption band of water. The lab-made Raman shifter cell, with a path length of 1 m, is filled with deuterium gas at 650 psi. Both forward and backscattered beams from the Raman shifter are directed toward the sample from two sides to yield a more uniform longitudinal heating pattern. Polarization of one of these beams is rotated by 90° to avoid standing wave and Bragg grating formation inside the sample. The sample temperature after the jump is monitored over time by probing changes in water IR absorption at 1460 nm. The sample was heated in the irradiated spot with a 1.5 mm diameter by 5−10 K.

The excitation light, with a 2 mW incident power in a 10 nm FWHM band centered at a wavelength of 365 nm, is produced by the Black-LED-365 light source (Prizmatix, Southfield, MI), collimated and sharply (~0.7 mm diameter) focused in the center of the heated spot of the sample. The transmitted light is directed to a Silicon PIN photodiode (Thorlabs, Newton, NJ) that measures the absorption kinetics. The fluorescence emission is collected at an ~50° angle with a three-lens telescope with a narrow band interference filter in the parallel part of the beam and detected with a R4220P photomultiplier tube (Hamamatsu, Bridgewater, NJ). NADH fluorescence is selected by a 458 nm narrow-band filter (bandwidth of 40 nm FWHM; Andover, Salem, NH). The signals from the photomultiplier tube and the absorption channel photodiode, amplified with lab-made transimpedance preamplifiers with a 3 ns response time, are digitized with a PCI-5152 data acquisition board (National Instruments, Austin, TX). The incident intensity of the excitation beam and the transmitted intensity of the fast IR thermometer beam are measured with photodiodes (Thorlabs), and the signals are digitized with a PCIe-6251 data acquisition board (National Instruments). The LED source is triggered to open the excitation beam a few milliseconds before the heating pulse and close 1 ms after the end of data acquisition. The timing of all events is determined by a DG535 delay generator (Stanford Research Systems, Sunnyvale, CA) triggered from the Q-switch. The setup is computer-controlled using a lab-made program written in LabVIEW (National Instruments). The temperature jump kinetic response from the corresponding osmolyte solution, measured in a special series of experiments, was subtracted from the absorption kinetics.

Materials. Pig heart LDH (Roche Diagnostics, Indianapolis, IN) was dialyzed at 4 °C in an 8000 molecular weight cutoff SpectraPor 7 tube (Fisher Scientific, Pittsburgh, PA) against 0.1 M TEA buffer (≥99.0% pure, Sigma Chemical Co., St. Louis, MO) at pH 7.5 three times for 20−25 h in each run and then concentrated using Microcon YM-10, 10000 molecular weight cutoff regenerated cellulose filters (Millipore, Bedford, MA). NAD^+ free acid and NADH sodium salt, both Grad 1, 100% purity (Roche Diagnostics), L-lactate sodium salt (98% pure, Sigma Chemical Co.), pyruvate monosodium salt (Boehringer, Mannheim, Germany), trimethylamine *N*-oxide dihydrate (≥99% pure, Fluka), and urea (≥99% pure, Sigma Chemical Co.) were used as received. Fresh solutions of all reagents were prepared for each experiment.

As determined previously (*23*), significant changes in NADH are observed only when the reaction mixtures include excess lactate and NAD^+. In this study, the lactate concentration was 5 mM, which is well below the self-inhibition level of 26 mM (*24*), and the NAD^+ concentration was 0.4 mM, stoichiometric with LDH active sites. Within the time period of our studies, we did not see any traces of the NAD−pyruvate adduct that can be produced slowly at high concentrations of pyruvate (*20*). The resulting total concentration of NADH (Figure 2) increased from 140 to ~200 μM upon addition of TMAO, saturating at 1 M TMAO, but decreased upon addition of urea instead of TMAO, reaching 58 μM at 2 M urea. The system with 2 M urea did not show any reaction-related kinetic response, because of expected LDH unfolding.

RESULTS AND DISCUSSION

Laser-Induced Temperature Jump Kinetics. For the problem at hand, we are interested in how the dynamics of the

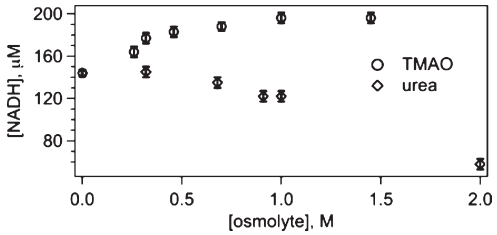

FIGURE 2: Total equilibrium concentration of produced NADH as a function of osmolyte concentration. Initial concentrations were as follows: 0.4 mN LDH (this refers to the molar concentration expressed in subunits of the tetrameric protein), 0.4 mM NAD^+, and 5 mM lactate.

binding and on enzyme chemistry of the pyruvate−lactate interconversion catalyzed by LDH, as given in the simplified scheme, are affected by the addition of osmolytes:

$$\mathrm{LDH\cdot NAD^+ + lactate} \underset{k_{-2}}{\overset{k_2}{\rightleftharpoons}} \mathrm{LDH^{OPEN}\cdot NAD^+\cdot lactate} \underset{k_{-3}}{\overset{k_3}{\rightleftharpoons}}$$

$$\mathrm{LDH^{CLOSED}\cdot NAD^+\cdot lactate} \underset{k_{-4}}{\overset{k_4}{\rightleftharpoons}}$$

$$\mathrm{LDH^{CLOSED}\cdot NADH\cdot pyruvate} \underset{k_{-5}}{\overset{k_5}{\rightleftharpoons}}$$

$$\mathrm{LDH^{OPEN}\cdot NADH\cdot pyruvate} \underset{k_{-6}}{\overset{k_6}{\rightleftharpoons}} \mathrm{LDH\cdot NADH + pyruvate} \quad (1)$$

The rate constant numbering and labeling pattern conforms with our previous study (*23*). The terms "open" and "closed" refer to the putative geometries of the surface mobile loop of the protein (residues 98−110). It is known that, in addition to the steps shown, NADH and NAD^+ both dissociate from LDH, lactate is known to inhibit the LDH·NADH complex at high concentrations, and pyruvate reacts slowly with the LDH·NAD^+ complex to form the protein-bound NAD−pyruvate adduct. The chemical conditions here were chosen to minimize these side reactions while maximizing observation of the chemical step.

Temperature jump relaxation spectroscopy is a quite useful approach to studying the kinetics of fast chemical reactions like the hydride transfer step of the LDH on enzyme interconversion of lactate to pyruvate or fast structural rearrangements of the enzyme·ligand system. In relaxation spectroscopy, fast steps can occur independent of slow steps under favorable conditions, and they are not necessarily masked by the slow steps. Moreover, the resolution available to our studies, ~20 ns, is quite sufficient to resolve even the fastest events. We have previously worked out the equilibrium conditions of the reacting system as a function of the concentration of LDH, NAD^+, and lactate (*23*). At high concentrations of the three species, excess lactate yields approximately equal amounts of species on the pyruvate and lactate sides of the reaction (Figure 2).

We report here temperature jump-induced changes in NADH fluorescence and absorption in the reaction system described above with initial concentrations of 0.4 mN LDH (this refers to the molar concentration of subunits of the tetrameric protein), 0.4 mM NAD^+, 5 mM lactate, and varying amounts of an osmolyte (TMAO or urea). The absorption kinetics reflects changes in the total amount of NADH (protein-bound and not bound), because the absorption spectrum of the nicotinamide moiety of NADH (maximum near 340 nm) is practically unaffected by

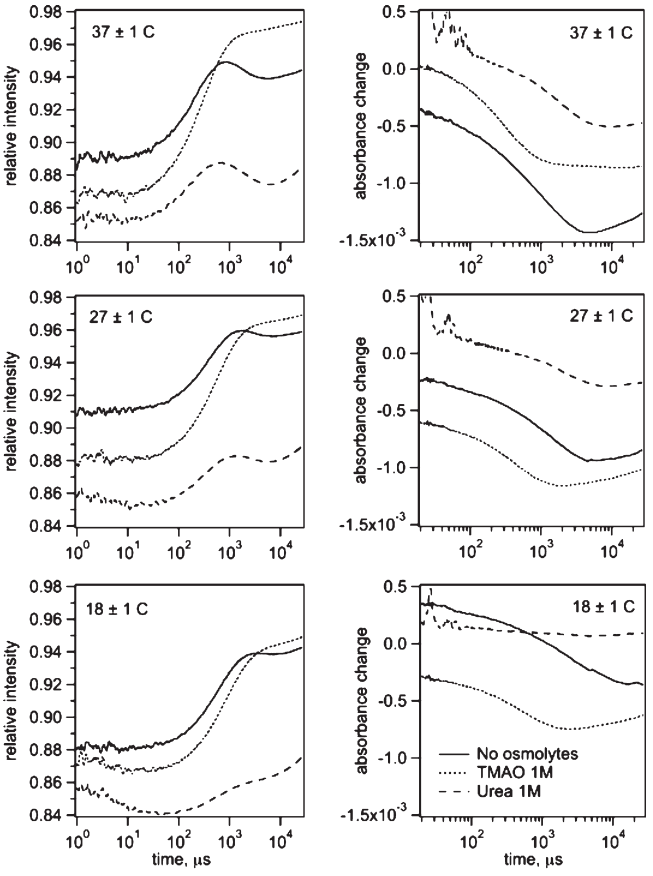

FIGURE 3: Fluorescence (left) and absorption (right) temperature jump kinetics of the reaction system: 0.4 mM LDH, 0.4 mM NAD^+, and 5 mM lactate (total initial concentrations) without osmolytes (—) or with 1 M TMAO (···) or 1 M urea (---). Spurious pulses below 100 μs arise from an artifact.

binding. On the other hand, fluorescence emission of NADH is very sensitive to enzyme and substrate binding. The NADH emission quantum yield strongly increases when NADH binds LDH and strongly decreases when pyruvate binds the LDH·NADH complex (*22*).

Temperature jump fluorescence kinetics without osmolytes (Figure 3) exhibit a strong increase in intensity in the time range of few hundred microseconds that originates mainly from pyruvate unbinding from the LDH·NADH complex (*22*, *23*). This increase is followed by a small intensity drop in the range of few milliseconds that is mainly determined by relaxations of chemical step and loop opening and closing (*23*). In the absorption kinetics, the dominating feature is a decrease in absorption due to a shift in the reaction equilibrium from the NADH side to the NAD^+ side.

In the presence of ≤1.4 M TMAO, the fluorescence kinetics significantly changes its profile: the submillisecond intensity rise becomes stronger, but the millisecond intensity drop becomes weaker. The shape and amplitude of the absorption kinetics do not change much, but a shift to shorter times is observed. Urea at concentrations of up to 1.0 M produces roughly the opposite effect on the shape of the fluorescence kinetics: the submillisecond rise becomes much weaker, while the millisecond drop becomes relatively stronger. In presence of urea, the amplitude of the absorption kinetic response becomes substantially smaller.

The kinetic measurements were conducted for a series of concentrations of TMAO or urea, and all data were preliminarily

analyzed using multiexponential fits. A preliminary analysis showed that the urea studies were not affected by protein unfolding, which was found for urea concentrations higher than used here. Detailed processing using computer simulations was performed for three systems: (a) without osmolytes, (b) with 1 M TMAO, and (c) with 1 M urea. The data processing was based on the kinetic model given by eq 1. In addition to the reaction steps shown, the binding of NAD^+ and NADH to LDH was included in the fits (given by rate constants k_1, k_{-1}, k_7, and k_{-7}, respectively, as in our previous study). We omitted here the surface mobile loop opening and closing steps without the substrate or product bound. Therefore, the on rate constants k_2 and k_{-6} incorporate the binding competence factor that is the fraction of loop open enzyme conformation. This minimal model for the analysis of protein dynamics contains 14 reaction rates. Some of them (k_1, k_{-1}, k_2, k_{-2}, k_7, and k_{-7}) affect the kinetics to a minor degree. Therefore, their values are based on literature data for similar experimental conditions, with slight adjustments to yield in our simulations the observed amounts of total NADH. The eight remaining kinetic rate constants are the unknowns. We used computer simulations, fitting the experimental data as described below to determine the microscopic rate constants of the individual reaction steps, basically in accord with our previous study (*23*).

Computer Simulation Procedure. Gepasi version 3.30 (*25*, *26*), a biochemical reaction simulation program, allows reconstruction, from known individual rate constants, of the kinetic response of a reaction system as it comes to equilibrium from a given initial state. The details of our simulation method were described previously (*23*). In short, the following procedure was used. To simulate each pair of fluorescence and absorption kinetics, we used a two-step process. First, the equilibrium concentrations of all reagents were found for the initial prejump temperature. Then, these results were used as starting parameters to find the time dependences of all concentrations on their approach to a new equilibrium at the new temperature after temperature jump; the simulated absorption and fluorescence kinetics were calculated from them, using NADH relative quantum yields taken from our previous studies (*22*, *23*). In every simulation step, some guess for the rate constants was used. The results from our previous study were taken as the initial guess for the very first simulation of the kinetics without an osmolyte. The rate constants for the loop dynamics, chemical step, and pyruvate binding and unbinding were adjusted to yield the best fit to the experimental kinetics, within the noise. From the resulting rate constants, the starting guess values for simulation of a temperature jump from the next temperature were determined by extrapolation or interpolation, and so on. For the experiments with osmolytes, the initial parameters were also slightly adjusted to yield the observed total concentrations of NADH produced in the reaction. These simulations were performed at four after-jump temperatures for the reaction system without osmolytes, for the system with 1 M TMAO, and for the system with 1 M urea. As we demonstrated previously (*23*), each of the addressed reaction steps determines some specific part of the fluorescence and/or absorption relaxation kinetics, and unequivocal evaluation of hydride transfer and pyruvate binding and unbinding rate constants is possible. Some overlap between the kinetic features for the loop dynamics on two sides of the reaction makes the corresponding rate constants (k_3, k_{-3}, k_5, and k_{-5}) slightly interdependent. Nonetheless, all these rate constants affect the reconstructed absorption and fluorescence relaxation kinetics with their own, well-distinguished patterns. Moreover,

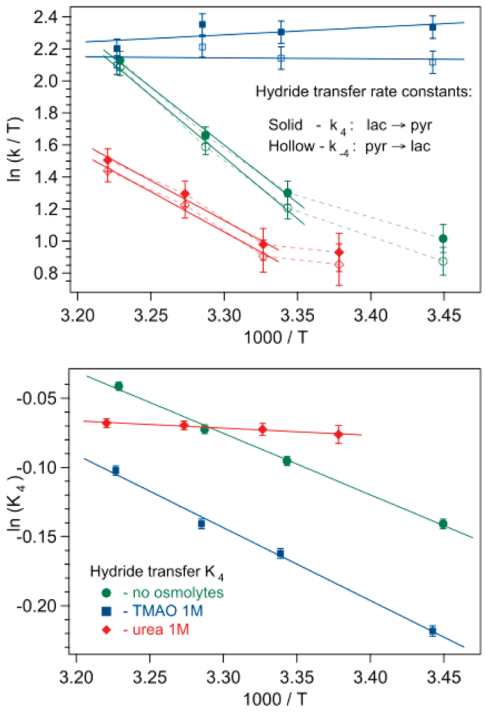

FIGURE 4: Hydride transfer rate constants in Eyring coordinates (top) and equilibrium constants in Arrhenius coordinates (bottom): without osmolytes, with 1 M TMAO, and with 1 M urea. In the top graph, solid symbols correspond to data for the forward reaction (from lactate to pyruvate) and empty symbols to data for the back reaction. Solid lines are linear fits. The error bars represent average parameter variances in near-successful iterations resulting in simulated kinetics with their difference being close to the noise level.

compared with our previous results (*23*), much lower noise in the absorption kinetics, due to a 2 order of magnitude higher light intensity used in this study, allowed much better evaluation of all rate constants. The simulation results are presented in Figures 4−7 as Eyring plots of the rate constants and Arrheniun plots of the equilibrium constants for the hydride transfer step, for loop dynamics with substrate/product·cofactor bound, and for pyruvate binding and unbinding. The error bars were determined from average parameter variances in near-successful iterations resulting in simulated kinetics with their difference being close to the noise level. The activation energies and enthalpy differences for the addressed reaction steps in the absence and presence of the osmolytes were determined from the slopes of the plots. The resulting values are listed in Tables 1−4 and summarized in Figure 8 as enthalpy profiles.

Hydride Transfer. Our previous work associated the kinetic events given by k_4 and k_{-4} with the hydride transfer chemical step based on a derived primary kinetic H−D isotope effect KIE of ~1.7 (*23*). The temperature behavior of the rate constants for the chemical step obtained from the simulations for the on-enzyme lactate to pyruvate (k_4) and pyruvate to lactate (k_{-4}) reactions in the system without osmolytes is shown in Eyring coordinates in the top panel of Figure 4. A similar pattern, but with a smaller slope, is observed with 1 M urea. The barrier height corresponding to the nearly linear higher-temperature part is approximately one-third lower with urea (Table 1). This certainly shows that in 1 M urea, the active site domain is distorted but not unfolded. The key interacting groups involved in the hydride transfer are still in their proper positions and in sufficiently close proximity to the substrate to catalyze chemistry. The system with 1 M TMAO shows a quite different pattern of behavior: the hydride transfer

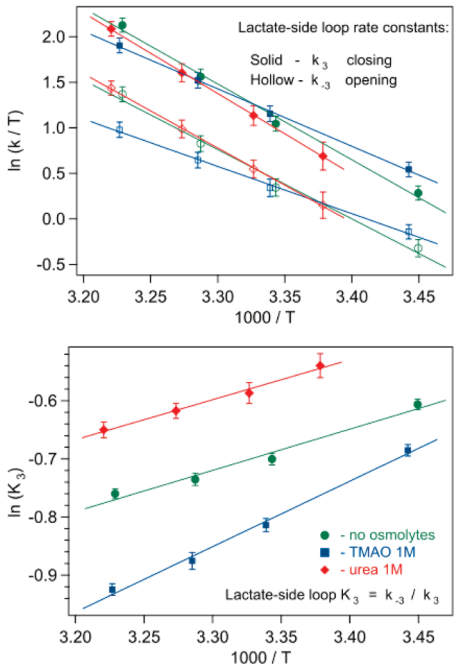

FIGURE 5: Effect of osmolytes on loop opening and closing rate constants with bound lactate·NAD^+, shown in Eyring coordinates (top). The bottom graph shows the loop equilibrium constants in Arrhenius coordinates. The error bars represent average parameter variances in near-successful iterations resulting in simulated kinetics with their difference being close to the noise level.

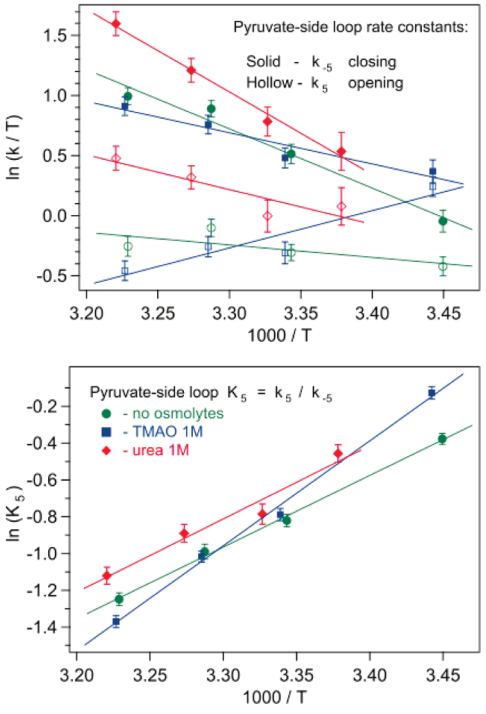

FIGURE 6: Effect of osmolytes on loop opening and closing rate constants with bound pyruvate·NADH, shown in Eyring coordinates (top). In the bottom graph, the loop equilibrium constant is plotted in Arrhenius coordinates. The error bars represent average parameter variances in near-successful iterations resulting in simulated kinetics with their difference being close to the noise level.

rate constants are close to the maximal, high-temperature values observed for the no-osmolyte system, and nearly independent of temperature over the whole range addressed. In general, hydride transfer rates are higher in TMAO and lower in urea than in the

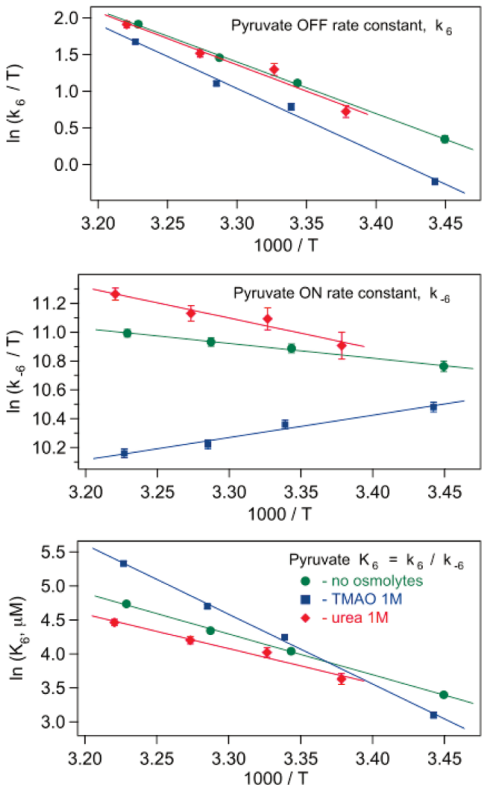

FIGURE 7: Effect of osmolytes on the pyruvate unbinding and binding rate constants (Eyring coordinates, top and middle) and the dissociation constant (Arrhenius coordinates, bottom). The error bars represent average parameter variances in near-successful iterations resulting in simulated kinetics with their difference being close to the noise level.

no-osmolyte system. Qualitatively, this is in accord with the presumed effect of these osmolytes: TMAO promotes compaction and protein stability, while urea works in the opposite direction. Strong enhancement of the enzymatic transfer of hydride from NADH due to high-pressure barrier compression, promoting tunneling through the transition state barrier or classical barrier traversal, has been observed experimentally (*27*, *28*).

The microscopic "equilibrium constant" ($K_4 = k_{-4}/k_4$) of the hydride transfer step (Figure 4, bottom panel) is close to unity in all cases, and the on-enzyme hydride transfer is almost isoenergetic: the enthalpy of on-enzyme conversion of lactate·NAD^+ to pyruvate·NADH is much lower than that in solution (NADH is a high-energy compound). Moreover, the energy levels of lactate·NAD^+ and pyruvate·NADH are inverted on enzyme, with the on-enzyme pyruvate·NADH energy slightly lower. A nearly linear Arrhenius dependence of K_4 is observed for all three systems: no osmolyte, TMAO, and urea. The corresponding enthalpy values are listed in Table 1. TMAO at a concentration of 1 M increases the hydride transfer enthalpy of K_4 by 18%. In 1 M urea, the enthalpy decreases substantially. It seems likely that the decrease and inversion of the enthalpy are the result of active site electrostatic interactions. These interactions presumably become stronger in TMAO because of compaction of the globule, yielding a stronger inversion of the hydride transfer enthalpy. Urea apparently produces the effect opposite to that of TMAO, expanding the protein globule and weakening the active site electrostatic interactions. This results in a decrease in the inverted hydride transfer enthalpy, almost to the crossover point.

Active Site Loop Dynamics. As shown in our previous studies (*22*, *23*), the tails of the absorption and fluorescence

Table 1: Hydride Transfer Barriers and Enthalpy Differences Obtained from Computer Simulations of Experimental Temperature Jump Kinetics[a]

	$\Delta H^{\ddagger}_{L}$ (kcal/mol)	$\Delta H^{\ddagger}_{P}$ (kcal/mol)	ΔH (kcal/mol)
no osmolyte	14.5 ± 1.6	15.5 ± 1.5	0.89 ± 0.04
1 M TMAO	−1.0 ± 0.9	0.0 ± 0.9	1.05 ± 0.05
1 M urea	9.6 ± 2.3	9.7 ± 2.3	0.10 ± 0.08

[a] $\Delta H^{\ddagger}_{L}$ is the enthalpy barrier height on the "lactate" side derived from the slope of the k_4 Eyring plot. $\Delta H^{\ddagger}_{P}$ is the enthalpy barrier height on the "pyruvate" side derived from the k_{-4} Eyring plot. Barrier heights for no-osmolyte and urea systems were calculated for the temperature range of 26−38 °C. ΔH is the enthalpy difference derived from the Arrhenius behavior of $K_4 = k_{-4}/k_4$.

Table 2: Active Site Loop Closing and Opening Barrier Heights and Enthalpy Differences ($\Delta H = H_{closed} - H_{open}$) with Bound Lactate·$NAD^+$[a]

	$\Delta H^{\ddagger}_{C}$ (kcal/mol)	$\Delta H^{\ddagger}_{O}$ (kcal/mol)	ΔH (kcal/mol)
no osmolyte	16.5 ± 1.0	15.2 ± 1.1	1.40 ± 0.11
1 M TMAO	12.5 ± 1.0	10.3 ± 1.0	2.23 ± 0.13
1 M urea	17.7 ± 1.9	16.4 ± 1.8	1.34 ± 0.28

[a] $\Delta H^{\ddagger}_{C}$ is the loop closing enthalpy barrier derived from the slope of the k_3 Eyring plot. $\Delta H^{\ddagger}_{O}$ is the loop opening enthalpy barrier derived from the k_{-3} Eyring plot. ΔH is the enthalpy difference derived from the Arrhenius behavior of $K_3 = k_{-3}/k_3$.

Table 3: Active Site Loop Closing and Opening Barrier Heights and Enthalpy Differences ($\Delta H = H_{closed} - H_{open}$) with Bound Pyruvate·NADH[a]

	$\Delta H^{\ddagger}_{C}$ (kcal/mol)	$\Delta H^{\ddagger}_{O}$ (kcal/mol)	ΔH (kcal/mol)
no osmolyte	9.7 ± 1.0	2.2 ± 1.0	7.8 ± 0.4
1 M TMAO	5.3 ± 1.1	−6.2 ± 1.1	11.3 ± 0.5
1 M urea	14.0 ± 2.0	6.2 ± 2.1	8.0 ± 0.8

[a] $\Delta H^{\ddagger}_{C}$ is the loop closing enthalpy barrier derived from the k_{-5} Eyring plot. $\Delta H^{\ddagger}_{O}$ is the loop opening enthalpy barrier derived from the k_5 Eyring plot. ΔH is the enthalpy difference derived from the Arrhenius behavior of $K_5 = k_5/k_{-5}$.

Table 4: Apparent Barrier Heights and Enthalpy Differences for Pyruvate Binding to the LDH·NADH Complex[a]

	$\Delta H^{\ddagger}_{OFF}$ (kcal/mol)	$\Delta H^{\ddagger}_{ON}$ (kcal/mol)	ΔH (kcal/mol)
no osmolyte	14.0 ± 0.5	2.0 ± 0.4	12.0 ± 0.4
1 M TMAO	17.3 ± 0.5	−3.1 ± 0.4	20.3 ± 0.5
1 M urea	14.1 ± 1.1	4.1 ± 1.1	9.8 ± 1.1

[a] $\Delta H^{\ddagger}_{OFF}$ is the enthalpy barrier derived from k_6. $\Delta H^{\ddagger}_{ON}$ is the enthalpy barrier derived from k_{-6}. ΔH is the enthalpy difference derived from the Arrhenius behavior of $K_6 = k_6/k_{-6}$.

kinetics after 0.5 ms depend significantly on the active site mobile loop dynamics (k_3, k_{-3}, k_5, and k_{-5}), and variation of each rate constant affects the kinetics in its own specific way. The simulation results show that for all three systems studied, in the temperature range of 15−37 °C, the mobile loop closing rate is 1.5−3 times higher than the opening rate for both LDH·NAD^+·lactate (Figure 5) and LDH·NADH·pyruvate (Figure 6) species. The loop is mainly in the closed conformation. It might be natural to expect that opening the loop requires additional energy, and the open/closed ratio would increase with temperature, becoming closer to unity. However, as in our previous study of this system (*23*), this ratio always decreases with temperature. This

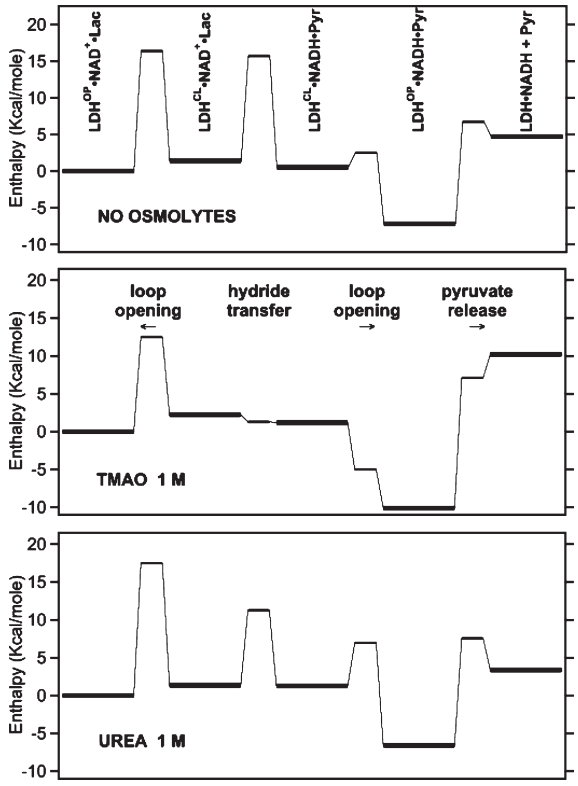

FIGURE 8: Enthalpy profiles for the hydride transfer, loop opening and closing, and pyruvate unbinding and binding reaction steps without osmolytes, with 1 M TMAO, and with 1 M urea. OP and CL refer to the loop open and closed geometries, respectively. The zero energy level is arbitrarily assigned to the lactate-side encounter complex (actually, this level must slightly differ for the three systems).

anti-Arrhenius temperature dependence, as proposed in our previous reports on substrate binding dynamics (*15*, *22*), appears to originate from partial unfolding required for the loop motions, which results in substantial entropy changes.

Addition of an osmolyte differently affects the loop behavior on two sides of the reaction. If lactate is bound to the LDH·NAD^+ complex, TMAO increases and urea slightly decreases the closed state preference (Figure 5). With 1 M TMAO, loop closing and opening rates increase 24 and 50%, respectively, while the closing and opening enthalpy barriers decrease 24 and 32%, respectively (Table 2). In urea, the loop rate constants do not change much, but both barriers increase by ∼7%. The loop closing enthalpy is not affected by 1 M urea and rises by ∼60% with TMAO.

On the pyruvate side, 1 M urea accelerates the loop motions (Figure 6), especially the closing rate at higher temperatures. The rate constants increase by 20−75% for closing and by ∼50% for opening. The enthalpy barrier heights (Table 3) increase in urea: the opening barrier is 2.8 times higher than without osmolytes, and the closing barrier is higher by ∼40%. The open/closed ratio for the LDH·NADH·pyruvate complex increases in urea by ∼20% uniformly, without any change in the loop closing enthalpy. The effect of TMAO is even more complicated. At lower temperatures (15−20 °C), the loop opening and closing rates are faster than those without osmolytes, but at higher temperatures (above 25−27 °C), they become slower. The loop closing barrier height decreases by 45% in 1 M TMAO, and the loop opening rate constant exhibits strongly non-Arrhenius behavior with negative apparent activation enthalpy. The loop closing enthalpy increases by 45%. Qualitatively, this all suggests that the loop

opening in the LDH·NADH·pyruvate complex requires stronger rearrangements around the active site and more significant entropy changes than without osmolytes, most probably because of the increased rigidity of the LDH backbone in TMAO.

Comparing the loop dynamics on the two sides of the reaction, we can also see that the loop opens and closes faster on the lactate side; the difference is greater at higher temperatures, and it increases even more upon addition of TMAO. This may be explained by additional steric hindrance in the LDH·NADH·pyruvate complex for the loop motion resulting from the hydrogen bond between Arg-109 located in the loop and the carbonyl group of pyruvate. There is no such hydrogen bond in the LDH·NAD^+·lactate complex because lactate is not structurally poised for it. At the same time, the barrier for loop opening is lower on the pyruvate side than on the lactate side: 2.2 kcal/mol versus 15.2 kcal/mol. Moreover, on both sides, TMAO decreases this barrier, and on the pyruvate side, TMAO even inverts the barrier. Apparently, the structural rearrangements required for loop motion in the LDH·NADH·pyruvate complex are more severe than in the LDH·NAD^+·lactate complex.

Pyruvate Release and Binding. The top panel in Figure 7 shows the temperature dependence of the rate constant (k_6) for the release of pyruvate from the LDH·NADH complex. With and without osmolyte, this rate constant demonstrates a good linear dependence in the Eyring coordinates. The resulting enthalpy barrier of ~14 kcal/mol is practically unchanged in 1 M urea (Table 4). For 1 M TMAO, the off rate is ~30% lower than without osmolyte, and the barrier is 24% higher. This is consistent with the assumed higher rigidity of the protein with added TMAO.

Compared to the no-osmolyte system, the apparent on rate constant [k_{-6} (middle panel of Figure 7)] increases with 1 M urea by 15−25%, but the apparent binding barrier becomes twice as high. The effect of TMAO is quite different: the pyruvate on rate decreases 1.5−2.3-fold, and its temperature dependence becomes inverse Arrhenius. Similar anti-Arrhenius behavior was observed for the binding of a pyruvate substrate analogue, oxamate, to the LDH·NADH complex (*15*, *22*).

Previous binding studies (*15*) of the LDH·NADH complex with oxamate in the presence of osmolytes showed that the protein binary complex exists in two conformational ensembles: one that is competent (denoted C) to bind the substrate analogue and one that is not (denoted NC). In the reaction kinetic scheme used here to analyze the data, we did not include the interconversion step between the competent and non-binding-competent forms. Therefore, assuming the same binding pathway for pyruvate as for oxamate, the observed rate constant is apparent, and the behavior shown in Figure 7 can be in fact represented as a product: $k_{ON\ App} = k_{ON}K_{C/NC}$, where k_{ON} is the actual on rate constant and the binding competence factor [$K_{C/NC} = c_C/(c_C + c_{NC})$] is the fraction of the LDH·NADH complex competent for pyruvate binding. The effect of temperature and osmolyte composition can modulate either factor. In those studies, it was found that the observed on rate followed both Arrhenius and inverse-Arrhenius behavior depending on the temperature range. The effects observed here for the on rate of pyruvate are qualitatively similar in that both normal Arrhenius as well as inverse Arrhenius behavior are observed. This reinforces our previous interpretation that the binding competent and incompetent LDH·NADH species differ in the rearrangement of low-energy hydrogen bonds as would arise from changes in internal hydrogen bonding and/or increases in the level of solvation of the protein structure (*15*, *29*).

CONCLUSIONS

It is a deep puzzle of how solutes affect protein structure and function. In general, numerous measurements have shown that the organic osmolyte, urea, increases K_m values of enzymes while the counteracting osmolyte, TMAO, decreases them (*5*, *10*, *30*). The fact that proteins populate a number and range of conformational substates, interconverting on virtually all time scales from femtoseconds to minutes and longer, that may differ in their biological function is well-established (although perhaps not so well appreciated given that static crystal structures of proteins, for example, tend to focus undue attention on average atomic positions). Mashino and Fridovich (*10*) hypothesized that TMAO affects protein function by shifting the conformational ensemble of the enzyme's native state to populate more compact conformers, while urea is shifting the native state ensemble in the opposite direction. Our recent studies on the effects of osmolytes on binding of substrate mimics to triosephosphate isomerase (*14*) and lactate dehydrogenase (*15*) showed not only that this was true but also that osmolytes affected the thermodynamics and interconversion kinetics of protein−ligand complexes.

Osmolytes, TMAO and urea, strongly affect the rates of specific events along the LDH-catalyzed reaction: binding of substrates, loop closure, and the chemical event. The core process of this reaction, transfer of a hydride between the C2 atom of the substrate (lactate or pyruvate) and the C4 atom of the cofactor (NAD^+ or NADH), is strongly enhanced by TMAO. Urea, on the other hand, decreases the rates substantially and shifts the hydride transfer enthalpy, normally inverted with respect to that in solution, almost to zero. The chemical rate increase caused by LDH is pretty well approximated by two, largely independent, molecular factors: (1) bringing the two interacting substrates close together in a reacting conformation and (2) strong electrostatic interactions between the lactate/pyruvate substrate and key active site residues, chiefly His-195, which stabilize the polar transition state of the reaction. Both factors would manifest in the ground state of the reaction complex by causing shortening of the distance between key interacting groups. We have shown that the LDH·NADH·oxamate (substrate analogue) Michaelis complex of LDH consists of an ensemble of interconverting (on time scales faster than the chemical rate) conformations, some much more reactive than others, as judged by the variation within the ensemble of the distances between the key groups (*31*).

Osmolyte-induced shifts in the conformational nature of the protein ensemble have been understood by studies (*8*, *11*) showing that TMAO has an unfavorable and urea a favorable interaction with the peptide backbone of proteins. TMAO suppresses the native state structural fluctuations, while urea enhances them. These effects occur with all proteins, resulting in TMAO-induced shifts in the native state to a more compact ensemble, and urea-induced shifts result in a more flexible and dynamic native ensemble. Provided that reaction competent species are associated with more compact and reaction incompetent with less compact conformations, which seems reasonable given the molecular mechanism of the chemical step in LDH, their effects on the catalytic step would be as measured. On the other hand, the observed effect of TMAO and urea on the apparent pyruvate binding rate constant suggests that more compact conformations are more likely to be incompetent with respect to substrate binding, while a moderate shift to less compact conformations increases the population of binding competent species. This shows that the effect of the osmolytes on the overall enzyme

activity is dependent on counteracting factors, and not straightforward.

REFERENCES

1. Yancey, P. H., Clark, M. E., Hand, S. C., Bowlus, R. D., and Somero, G. N. (1982) Living with water stress: Evolution of osmolyte systems. *Science 217*, 1214–1222.
2. Yancey, P. H., and Siebenaller, J. F. (1999) Trimethylamine oxide stabilizes teleost and mammalian lactate dehydrogenases against inactivation by hydrostatic pressure and trypsinolysis. *J. Exp. Biol. 202*, 3597–3603.
3. Lin, T. Y., and Timasheff, S. N. (1994) Why do some organisms use a urea-methylamine mixture as osmolyte? Thermodynamic compensation of urea and trimethylamine N-oxide interactions with protein. *Biochemistry 33*, 12695–12701.
4. Wang, A., and Bolen, D. W. (1997) A naturally occurring protective system in urea-rich cells: Mechanism of osmolyte protection of proteins against urea denaturation. *Biochemistry 36*, 9101–9108.
5. Yancey, P. H., and Somero, G. N. (1979) Counteraction of urea destabilization of protein structure by methylamine osmoregulatory compounds of elasmobranch fishes. *Biochem. J. 183*, 317–323.
6. Arakawa, T., and Timasheff, S. N. (1985) The stabilization of proteins by osmolytes. *Biophys. J. 47*, 411–414.
7. Bolen, D. W. (2001) Protein stabilization by naturally occurring osmolytes. *Methods Mol. Biol. 168*, 17–36.
8. Qu, Y., and Bolen, D. W. (2003) Hydrogen exchange kinetics of RNase A and the urea:TMAO paradigm. *Biochemistry 42*, 5837–5849.
9. Doan-Nguyen, V., and Loria, J. P. (2007) The effects of cosolutes on protein dynamics: The reversal of denaturant-induced protein fluctuations by trimethylamine N-oxide. *Protein Sci. 16*, 20–29.
10. Mashino, T., and Fridovich, I. (1987) Effects of urea and trimethylamine-N-oxide on enzyme activity and stability. *Arch. Biochem. Biophys. 258*, 356–360.
11. Qu, Y., Bolen, C. L., and Bolen, D. W. (1998) Osmolyte-driven contraction of a random coil protein. *Proc. Natl. Acad. Sci. U.S.A. 95*, 9268–9273.
12. Baskakov, I., Wang, A., and Bolen, D. W. (1998) Trimethylamine-N-oxide counteracts urea effects on rabbit muscle lactate dehydrogenase function: A test of the counteraction hypothesis. *Biophys. J. 74*, 2666–2673.
13. Yancey, P. H., and Siebenaller, J. F. (1987) Coenzyme binding ability of homologs of M4-lactate dehydrogenase in temperature adaptation. *Biochim. Biophys. Acta 924*, 483–491.
14. Gulotta, M., Qiu, L., Desamero, R., Rosgen, J., Bolen, D. W., and Callender, R. (2007) Effects of cell volume regulating osmolytes on glycerol 3-phosphate binding to triosephosphate isomerase. *Biochemistry 46*, 10055–10062.
15. Qiu, L., Gulotta, M., and Callender, R. (2007) Lactate dehydrogenase undergoes a substantial structural change to bind its substrate. *Biophys. J. 93*, 1677–1686.
16. Burgner, J. W., II, and Ray, W. J., Jr. (1984) On the origin of the lactate dehydrogenase induced rate effect. *Biochemistry 23*, 3636–3648.
17. Burgner, J. W., II, and Ray, W. J., Jr. (1984) The lactate dehydrogenase catalyzed pyruvate adduct reaction: Simultaneous general acid-base catalysis involving an enzyme and an external catalyst. *Biochemistry 23*, 3626–3635.
18. Burgner, J. W., II, and Ray, W. J., Jr. (1984) Acceleration of the NAD cyanide adduct reaction by lactate dehydrogenase: The equilibrium binding effect as a measure of the activation of bound NAD. *Biochemistry 23*, 3620–3626.
19. Deng, H., Zhadin, N., and Callender, R. (2001) Dynamics of protein ligand binding on multiple time scales: NADH binding to lactate dehydrogenase. *Biochemistry 40*, 3767–3773.
20. Gulotta, M., Deng, H., Deng, H., Dyer, R. B., and Callender, R. H. (2002) Toward an understanding of the role of dynamics on enzymatic catalysis in lactate dehydrogenase. *Biochemistry 41*, 3353–3363.
21. McClendon, S., Vu, D. M., Clinch, K., Callender, R., and Dyer, R. B. (2005) Structural transformations in the dynamics of Michaelis complex formation in lactate dehydrogenase. *Biophys. J. 89*, L07–L09.
22. McClendon, S., Zhadin, N., and Callender, R. (2005) The approach to the Michaelis complex in lactate dehydrogenase: The substrate binding pathway. *Biophys. J. 89*, 2024–2032.
23. Zhadin, N., Gulotta, M., and Callender, R. (2008) Probing the role of dynamics in hydride transfer catalyzed by lactate dehydrogenase. *Biophys. J. 95*, 1974–1984.
24. Holbrook, J. J., Liljas, A., Steindel, S. J., and Rossmann, M. G. (1975) Lactate Dehydrogenase. In The Enzymes, pp 191−293, Academic Press, New York.
25. Mendes, P. (1993) GEPASI: A software package for modelling the dynamics, steady states and control of biochemical and other systems. *Comput. Appl. Biosci. 9*, 563–571.
26. Mendes, P. (1997) Biochemistry by numbers: Simulation of biochemical pathways with Gepasi 3. *Trends Biochem. Sci. 22*, 361–363.
27. Hay, S., and Scrutton, N. S. (2008) Incorporation of hydrostatic pressure into models of hydrogen tunneling highlights a role for pressure-modulated promoting vibrations. *Biochemistry 47*, 9880–9887.
28. Hay, S., Sutcliffe, M. J., and Scrutton, N. S. (2007) Promoting motions in enzyme catalysis probed by pressure studies of kinetic isotope effects. *Proc. Natl. Acad. Sci. U.S.A. 104*, 507–512.
29. Pineda, J. R. E. T., Callender, R., and Schwartz, S. D. (2007) Ligand Binding and Protein Dynamics in Lactate Dehydrogenase. *Biophys. J. 93*, 1474–1483.
30. Hochachka, P. W., and Somero, G. N. (2002) Water-Solute Adaptions (Chapter 6). In Biochemical Adaptation, p 466, Oxford University Press, Oxford, U.K.
31. Deng, H., Brewer, S., Vu, D. M., Clinch, K., Callender, R., and Dyer, R. B. (2008) On the pathway of forming enzymatically productive ligand-protein complexes in lactate dehydrogenase. *Biophys. J. 95*, 804–813.